Crystal and Magnetic Structures of Layer Transition Metal Phosphate Hydrates

Simon G. Carling,[†] Peter Day,*[,†] and Dirk Visser[‡]

The Royal Institution, 21 Albemarle Street, London W1X 4BS, U.K., and Physics Department, Loughborough University of Technology, Loughborough, Leicestershire, U.K.

Received November 20, 1994[⊗]

$NH_4M^{II}PO_4 \cdot H_2O$ (M^{II} = Mn, Fe, Co, Ni) and $KM^{II}PO_4 \cdot H_2O$ (M^{II} = Mn, Co, Ni) have been prepared and characterized by X-ray powder diffraction and bulk magnetometry, and the corresponding deuterio compounds, by neutron powder diffraction. They are isomorphous (space group $Pmn2_1$). The divalent metal ions form approximately square-planar layers of corner-sharing octahedra, the layers being bound by hydrogen bonds in the ammonium compounds and by electrostatic interactions in the potassium ones. In all cases, the $M^{II}O_6$ octahedra are severely distorted, the point symmetry being C_{2v}. Bulk susceptibility measurements on $NH_4FePO_4 \cdot H_2O$, $NH_4MnPO_4 \cdot H_2O$, and $KMnPO_4 \cdot H_2O$ show they are weakly ferromagnetic, with Neel temperatures of T_N = 24.0(2), 17.5(3), and 18.0(3) K, respectively. Powder neutron diffraction was used to determine the underlying antiferromagnetic component of the structures. All three materials have simple two-sublattice structures, with the antiferromagnetic moments along ±[010], perpendicular to the plane of the metal-containing layers. Analysis using the irreducible representations of the space group shows that the ferromagnetic moments are parallel to [001].

Introduction

In the last 20−30 years, many compounds have been synthesized in which magnetic interactions between transition metal ions are essentially confined to one or two dimensions. They have served as model compounds on which the predictions of theory could be tested and refined. For example, among two-dimensional (2D) compounds, the layer perovskites $M^I_2M^{II}X_4$, which adopt structures based on the K_2NiF_4 lattice, have proved a rich source of model magnetic systems. In this structure, layers of corner-sharing $M^{II}X_6$ octahedra are separated by the monovalent cation, leading to much stronger exchange within the layers than between them. Thus for instance, K_2MnF_4 is a 2D antiferromagnet while K_2CuF_4 is a 2D ferromagnet.[1]

All compounds of the K_2NiF_4 series are of relatively high symmetry, and the exchange is mediated by monoatomic anions. In more recent years, a variety of 2D magnets with structural types other than layer perovskite have been studied. An example is the formate $Cu(HCO_2)_2 \cdot 4H_2O$,[2] which behaves as a square-planar Heisenberg antiferromagnet. This compound is monoclinic, and the exchange is mediated by the formate ion. Other examples of magnetic model compounds in which the exchange pathway is provided by complex ions include $BaM^{II}_2(PO_4)_2$ and $BaM^{II}_2(AsO_4)_2$ (M^{II} = Co, Ni), which were among the first compounds to be discovered that model the 2D XY magnet.[3] Another 2D XY system is M^INiAsO_4, where M^I = K, RNH_3.[4,5] The latter are structurally related to the layer silicates with the Ni ions forming honeycomb layers. A series of layered phosphates of similar formulas exist, although they adopt structures which differ from those of the arsenates.

An important goal of work on 2D magnetic model compounds has been to identify examples with spontaneous magnetization as a result of ferromagnetic near-neighbor exchange or ferrimagnetism. Ferromagnetic exchange in insulating solids is quite rare, though a few key cases such as K_2CuF_4[1] and the $A^I_2CrX_4$ series[6] have emerged. Much less explored as a source of finite zero-field magnetization is the phenomenon of spin canting. When the ligand field around an open-shell metal ion is of sufficiently low symmetry, so-called[7] antisymmetric exchange may occur between neighboring centers, which competes with collinear antiferromagnetism. This phenomenon leads to non-collinear order, which therefore results in an uncompensated resultant moment in one direction. A fruitful source of magnetic systems based on low-symmetry metal ion sites is provided by compounds in which the magnetic exchange is mediated by polyatomic anions. We have therefore chosen to investigate a series of ternary transition metal phosphates, which also contain coordinated water. As indicated below, these compounds all have pronounced layer crystal structures with the 3d ions occupying strongly distorted octahedral sites.

Ammonium phosphates of general formula $NH_4M^{II}PO_4 \cdot H_2O$ were first described in 1864 by Debray.[8] The series of phosphates $M^IM^{II}PO_4 \cdot H_2O$ (M^I = K, NH_4; M^{II} = Mg, Mn, Fe, Co, Ni) was reported by Bassett and Bedwell in 1933.[9] Infrared spectroscopic measurements[10] showed that the ammonium compounds contained coordinated water and ammonium ions, instead of having the alternative composition $M^{III}HPO_4 \cdot NH_3 \cdot H_2O$. The crystal structure of $NH_4CoPO_4 \cdot H_2O$ was determined by Tranqui in 1968[11] using powder X-ray diffraction. The unit cell parameters of the remaining compounds in the series were reported in the same year.[12] All these compounds were said to

* To whom correspondence should be addressed.
† The Royal Institution.
‡ Loughborough University of Technology.
⊗ Abstract published in *Advance ACS Abstracts,* June 15, 1995.

(1) de Jongh, L. J.; Miedema, A. R. *Adv. Phys.* **1974**, *23*, 1.
(2) Koyama, K.; Nobumasa, H.; Matsuura, M. *J. Phys. Soc. Jpn.* **1987**, *56*, 1553.
(3) Regnault, L. P.; Rossat-Mignod, J.; Henry, J. Y.; de Jongh, L. P. *J. Magn. Magn. Mater.* **1983**, *31−34*, 1205.
(4) Buckley, A. M. Thesis (Part II), University of Oxford, 1985.
(5) Buckley, A. M.; Bramwell, S. T.; Visser, D.; Day, P. *J. Solid State Chem.* **1987**, *69*, 240.
(6) For a review, see: Bellitto, C.; Day, P. *J. Mater. Chem.* **1992**, *2*, 265.
(7) Moriya, T. *Phys. Rev.* **1960**, *120*, 91.
(8) Debray. *C. R. Acad. Sci.* **1864**, *59*, 40.
(9) Basset, H.; Bedwell, W. L. *J. Chem. Soc.* **1933**, 137.
(10) Fraissard, J.; Etienne, J. J. *Bull. Soc. Fr. Mineral. Cristallogr.* **1967**, *90*, 162.
(11) Tranqui, D.; Durif, A.; Guitel, J.-C.; Averbuch-Pouchot, M. T. *Bull. Soc. Fr. Mineral. Cristallogr.* **1968**, *91*, 10.
(12) Durif, A.; Averbuch-Pouchot, M. T. *Bull. Soc. Fr. Mineral. Cristallogr.* **1968**, *91*, 495.

0020-1669/95/1334-3917$09.00/0

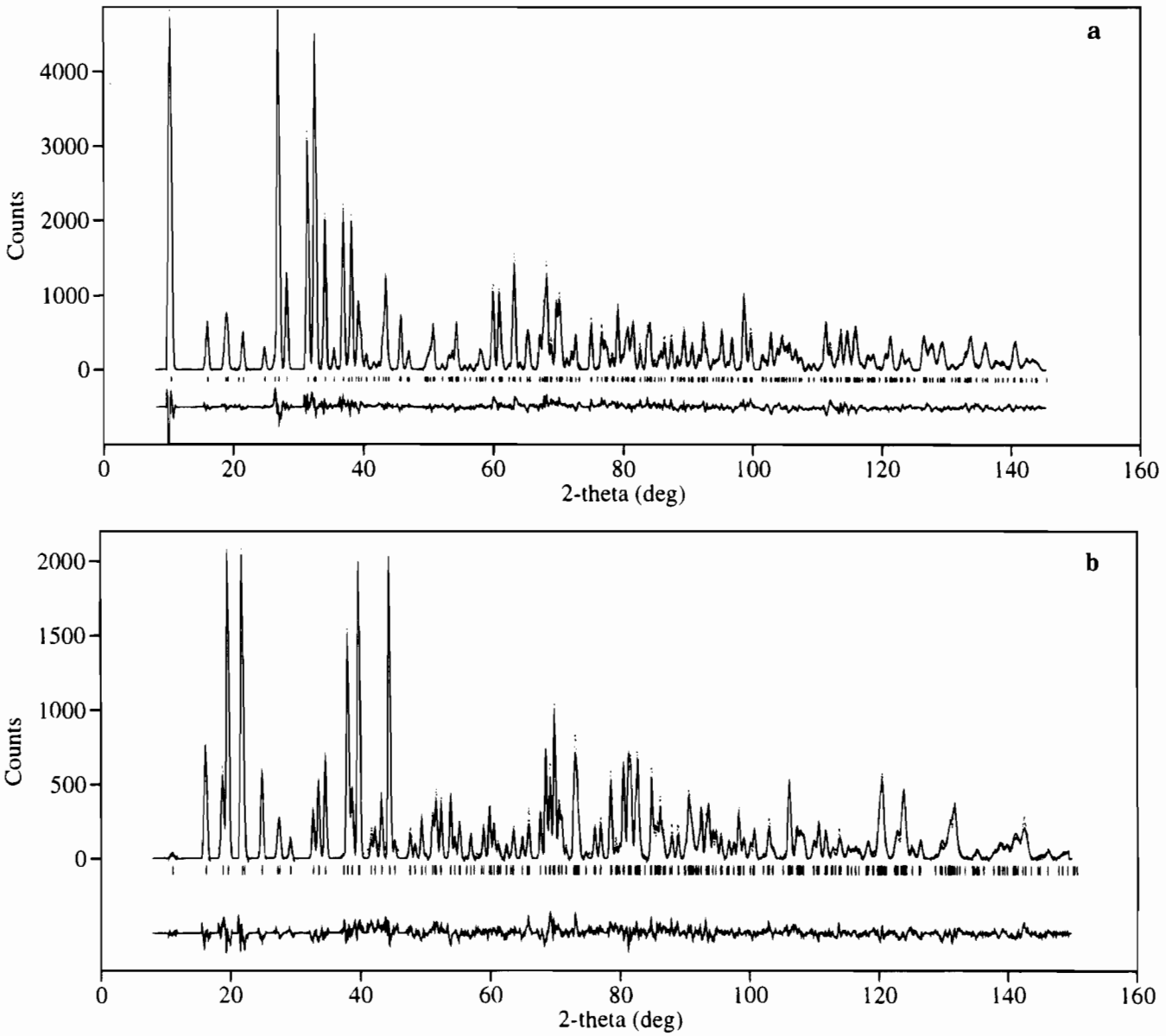

Figure 1. Observed (points), calculated (upper full line), and difference (lower full line) neutron powder diffraction profiles of (a) $ND_4MnPO_4{\cdot}D_2O$ and (b) $KMnPO_4{\cdot}H_2O$ at room temperature. Bars indicate calculated reflections.

crystallize in the orthorhombic space group $Pmn2_1$. The structure consists of approximately square-planar sheets of M^{II} ions, coordinated in a severely distorted octahedron by five phosphate oxygens and one water molecule, separated by the monovalent cation. The point symmetry at the metal ion sites corresponding to the symmetry of the space group is C_{2v}. One member of the series, $NH_4FePO_4{\cdot}H_2O$, has been shown to be weakly ferromagnetic below 26 K.[13] Mössbauer measurements led to the conclusion that the transition from the paramagnetic to the ordered phase was of first order. Bulk magnetic measurements on oriented polycrystalline samples showed significant anisotropy, especially below 80 K. Villeneuve *et al.*[14] reported bulk susceptibility and specific heat measurements on $NH_4CoPO_4{\cdot}H_2O$ and EPR measurements on $NH_4(Mg,Co)PO_4{\cdot}H_2O$ with a 5% doping level of Co. Both the specific heat and the observed splitting of the EPR signal were consistent with a 2D $S = {}^1/_2$ XY antiferromagnet.

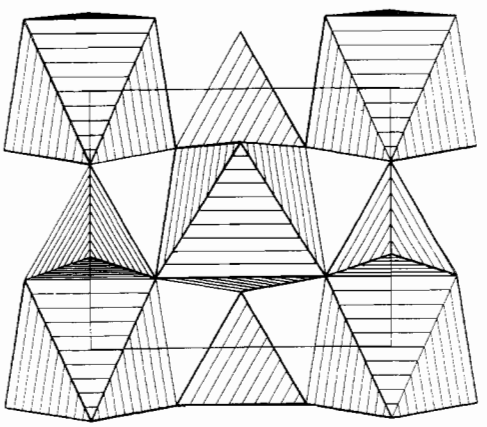

Figure 2. The $M^{II}PO_4{-}D_2O$ layer in $M^IM^{II}PO_4{\cdot}H_2O$ projected along (010).

This paper reports a full determination of the crystal structures of the compounds $M^IM^{II}PO_4{\cdot}H_2O$, with M^I = K, NH_4^+ and M^{II} = Mn, Fe, Co, Ni, including the elucidation of the nature of hydrogen bonding between the layers in the ammonium compounds, by means of powder neutron diffraction. We have

(13) Greedan, J. E.; Reubenbauer, K.; Birchall, T.; Ehlert, M.; Corbin, D. R.; Subramanian, M. A. *J. Solid State Chem.* **1988**, *77*, 376.
(14) Villeneuve, G.; Pizarro, J. L.; Dance, J. M.; Arriortua, M. I.; Roho, T.; Kuentzler, R. *J. Magn. Magn. Mater.* **1990**, *83*, 478.

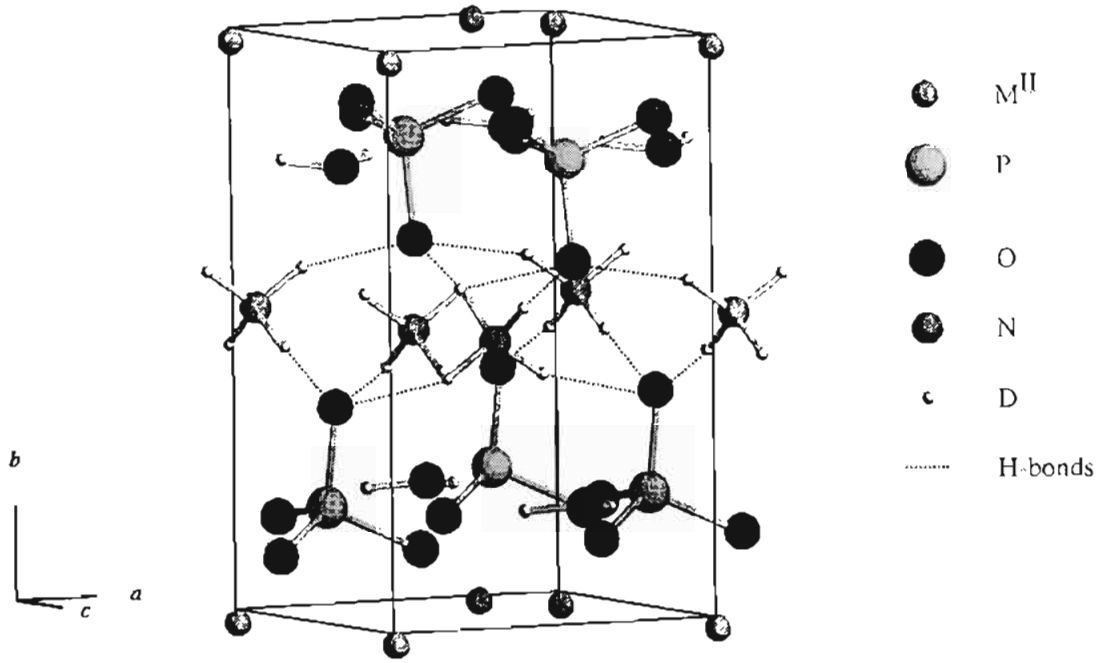

Figure 3. Crystal structure of $ND_4M^{II}PO_4{\cdot}D_2O$ showing the hydrogen bonds between ammonium and phosphate groups.

Table 1. Unit Cell Constants (Å) and Neutron Powder Diffraction Profile Refinement Parameters of $ND_4M^{II}PO_4{\cdot}D_2O$

M^{II}	*T*/K	*a*	*b*	*c*	R_{wp}	R_{exp}	R_I
Mn	1.6	5.7173(1)	8.8312(2)	4.8774(1)	9.73	2.70	6.77
	21.4	5.7142(1)	8.8255(2)	4.8762(1)	5.18	1.57	4.83
	295	5.7302(1)	8.8191(2)	4.9087(1)	10.67	3.29	6.35
Fe	1.4	5.6500(1)	8.8276(2)	4.8030(1)	10.48	2.99	6.79
	29.4	5.6490(1)	8.8215(1)	4.8011(1)	10.52	3.49	6.41
	295	5.6656(1)	8.8213(2)	4.8314(1)	10.01	3.34	7.08
Co	9.8	5.6082(1)	8.7902(1)	4.773(1)	8.60	2.03	4.98
	80	5.6110(1)	8.7906(2)	4.780(1)	11.55	4.21	7.16
	295	5.6247(1)	8.7795(2)	4.8022(1)	13.56	6.21	8.44
Ni	9.8	5.5576(1)	8.7684(2)	4.7312(1)	7.89	2.36	3.51
	80	5.5611(2)	8.7724(4)	4.7348(2)	9.10	1.41	7.91
	295	5.5735(2)	8.7597(2)	4.7517(1)	9.65	2.02	4.35

also investigated the magnetic ordering in these compounds by bulk susceptibility measurements and the magnetic structures by neutron diffraction. Brief preliminary notes of part of this work have appeared.[15]

Experimental Section

Synthesis. Unless otherwise stated, starting materials were of analytical grade and were used without further purification. Deuterated starting materials obtained from MSD Isotopes contained at least 99.5 atom % deuterium, with the exception of sulfuric acid-d_2, which contained only 96 atom % deuterium. D_2O was supplied by Aldrich Chemical Co., Inc., and was 99.9 atom % deuterium.

Ammonium and Deuterioammonium Salts. $NH_4M^{II}PO_4{\cdot}H_2O$ (M^{II} = Mn, Fe, Co, Ni) were prepared by precipitation from aqueous solution using a method derived from that of Bassett and Bedwell.[9] An approximately 0.5 M solution of a metal salt—the sulfate in the case of Fe, sulfate or chloride for Mn, and the chloride for Co and Ni—was added to an approximately 10 M excess of saturated $(NH_4)_2HPO_4$ solution. The resulting precipitate was digested at 85 ± 5 °C for 24–48 h, after which the microcrystalline product was filtered off and washed with deionized water. Finally the washed product was dried *in vacuo*. In the preparation of $NH_4MnPO_4{\cdot}H_2O$ or $NH_4FePO_4{\cdot}H_2O$, $(N_2H_6)SO_4$ was added to all solutions in order to prevent aerobic oxidation of the divalent metal ion under the extremely basic conditions. Since the damp products of these two metals are also prone to oxidation, the filtration was carried out under nitrogen.

Deuterated analogues of the ammonium metal phosphate hydrates were prepared by the method described for the hydrogenous compounds with several modifications. All manipulations of solutions or damp products were performed in a glovebox purged with dry nitrogen. The metal salt was dehydrated by heating *in vacuo* to remove any hydrogenous water of crystallization before being dissolved in D_2O. $(ND_4)_2DPO_4$ solution was prepared *in situ* by neutralizing D_3PO_4 solution in D_2O with ND_3 (26% in D_2O). Products were filtered off under nitrogen and dried *in vacuo*. Hydrazinium-d_6 sulfate was prepared by neutralization of hydrazine-d_4 solution in D_2O with sulfuric acid-d_2.

Potassium Salts. $KM^{II}PO_4{\cdot}H_2O$ (M^{II} = Mn, Co, Ni) were prepared by a method similar to that described above for the ammonium compounds; however, a larger excess of K_2HPO_4 solution was required, typically 15–20 M. The digestion period was longer, usually 48–60 h. Attempts to prepare $KFePO_4{\cdot}H_2O$ were not successful, as the product proved too susceptible to oxidation.

To synthesize $KM^{II}PO_4{\cdot}D_2O$, a solution of K_2DPO_4 was prepared by heating $K_2HPO_4{\cdot}3H_2O$ *in vacuo* to drive off the water of crystallization and then dissolving the dry salt in D_2O. D_2O solutions of the divalent metal salts were prepared in a similar manner, and the solutions were mixed under nitrogen in a glovebox. The precipitate was digested under reflux at 80 ± 5 °C for approximately 72 h, and the resulting product was filtered off under nitrogen and dried *in vacuo*.

Characterization. Elemental Analysis. Metal analyses were carried out by atomic absorption spectroscopy, and C, H, N were determined by combustion. Satisfactory results were obtained for all compounds.

Powder X-ray Diffraction. Powder X-ray diffraction profiles were recorded by using Cu Kα radiation and a Philips PW1710 diffractometer. Samples were mounted on aluminum plates; in the case of deuterated compounds, an air-sensitive cell was used and the sample loaded under nitrogen. Unit cell refinement was then carried out with the Dragon and Cellref or with the DSPA and Refcel programs. The observed reflections were indexed on an orthorhombic unit cell of space group $Pmn2_1$.

Powder Neutron Diffraction. Constant-wavelength neutron diffraction experiments were performed at the High Flux Reactor of the Institut Laue-Langevin, Grenoble, France, on the instruments D2B and D1B. The high-resolution powder diffractometer D2B[16] is a moving-

(15) Carling, S. G.; Day, P.; Visser, D. *Acta Crystallogr.* **1990**, *A46*, (suppl.), C-278; *J. Appl. Phys.* **1991**, *69*, 6016.

(16) *Guide to Neutron Research Facilities at the ILL*; ILL: Grenoble, France, 1988.

Table 2. O−M^{II}−O (α, β, γ, δ) and O−P−O (ϵ, ζ, η, κ) Bond Angles (deg) in $ND_4M^{II}PO_4{\cdot}D_2O$ as a Function of Temperature[a]

M^{II}	*T*/K	α	β	γ	(α + 2β + γ)	δ	ϵ	ζ	η	κ
Mn	1.6	66.2(2)	97.4(2)	98.9(3)	359.9(9)	175.3(4)	108.7(6)	111.8(4)	109.1(4)	106.2(4)
	21.4	67.0(2)	97.3(1)	98.4(2)	360.0(6)	177.1(3)	108.5(5)	111.3(3)	109.7(3)	106.4(4)
	298	65.0(2)	97.5(1)	100.1(2)	360.1(6)	175.2(3)	109.6(5)	110.3(3)	109.9(3)	106.9(4)
Fe	1.5	67.1(1)	95.7(1)	101.6(1)	360.1(4)	174.7(2)	109.6(3)	111.6(2)	109.9(2)	104.1(2)
	29.6	66.7(1)	95.6(1)	102.2(1)	360.1(4)	173.6(2)	109.7(3)	111.1(2)	110.2(2)	104.6(3)
	298	68.9(3)	95.8(2)	99.5(4)	360(1)	176.7(5)	108.8(6)	111.9(4)	109.7(4)	104.7(5)
Co	9.8	69.0(1)	95.9(1)	99.3(2)	360.1(5)	177.2(3)	108.9(4)	111.9(2)	110.1(3)	103.9(3)
	80	68.8(3)	95.9(2)	99.4(4)	360(1)	176.8(5)	108.8(6)	110.2(5)	110.6(4)	106.6(5)
	298	68.9(2)	95.5(2)	100.1(3)	360.0(9)	177.1(4)	109.0(5)	111.5(4)	110.2(3)	104.4(4)
Ni	9.8	69.5(1)	95.6(1)	99.2(1)	359.9(4)	176.3(2)	108.6(3)	111.8(2)	110.2(2)	104.3(2)
	80	69.6(2)	95.7(2)	99.0(2)	360.0(8)	177.3(3)	110.3(6)	111.0(4)	110.8(4)	102.9(5)
	298	69.2(2)	95.7(1)	99.5(2)	360.1(6)	176.5(3)	108.0(4)	112.2(3)	109.1(3)	106.2(4)

[a] For definition of angles, see Figure 4.

counter instrument using thermal neutrons monochromated to a wavelength of 1.5942 Å by a composite squashed Ge monochromator with a 135° takeoff angle. A multidetector bank containing 64 5-atm ^{3}He detectors spaced at 2.5° intervals in a B_4C resin is located 1 m from the sample position. The detectors have individual soller slit collimation.

D1B is a very-high-flux, medium-resolution powder diffractometer designed for thermodiffractometry and the solution of magnetic structures in low-moment systems.[17] A pyrolitic graphite monochromator gives a neutron wavelength of 2.52 Å, and a curved ^{3}He/Xe multidetector with 400 active elements collects data at a resolution of 0.2° over a 2θ range of 80°.

Magnetic Measurements. Magnetic measurements were carried out on polycrystalline samples using two SQUID magnetometers, a CCL S600 instrument at the Inorganic Chemistry Laboratory, Oxford, and a Quantum Design MPMS7 at the Royal Institution.

Results

Structural Refinements. Crystal structures of the ternary transition metal phosphate hydrates were refined from the neutron powder diffraction profiles by the Rietveld method,[18] using PROF1 and PROF2 programs,[19,20] PROFIL suite,[21] and the Los Alamos GSAS package.[22] Magnetic structures were refined using PROF1 and PROF2. Observed, calculated, and difference profiles for the room-temperature refinements of $ND_4MnPO_4{\cdot}D_2O$ and $KMnPO_4{\cdot}D_2O$ are shown in Figure 1. Corresponding data for the remaining compounds are available as supporting information.

The starting model for the structural refinements was taken from the structure determination of $NH_4CoPO_4{\cdot}H_2O$.[23] For the compounds $KM^{II}PO_4{\cdot}H_2O$, deuteron D was placed on a site of general symmetry in the structure such that the O(4)- -D bond length was 1 Å and the angle at the O(4) atom between D and its reflection in the *ab* mirror plane was 105°. The potassium ion K was positioned at the coordinates determined for the ammonium group. The deuterons of the ammonium group in the compounds $ND_4M^{II}PO_4{\cdot}D_2O$ were initially positioned as follows: two deuterons, D(1) and D(2), were placed on special positions in the *ab* mirror plane, with a third on a general site. All N−D bond lengths were set at 1 Å, and D−N−D angles were approximately 109°. (In the ammonium compounds, the water molecule deuteron is referred to as D(4).)

The compounds $ND_4M^{II}PO_4{\cdot}D_2O$ (M^{II} = Mn, Fe, Co, Ni) are isomorphous, crystallizing in space group $Pmn2_1$. No structural phase transitions were found below room temperature. The structure consists of puckered sheets of distorted, corner-sharing $M^{II}O_6$ octahedra, cross-linked by phosphate tetrahedra, as shown in Figure 2. These layers are separated by ammonium ions hydrogen-bonded to the apical phosphate oxygens. Figure 3 illustrates the layered nature of the structure and shows the hydrogen bonds between the ammonium and phosphate groups. The lengths of the hydrogen bonds are discussed later. The refinement of the structure of $ND_4MnPO_4{\cdot}D_2O$ at 21.4 K was complicated by the fact that the measured diffraction profile indicates that the sample retained a small amount of D_2O; extra peaks due to D_2O ice were therefore present in the profile. A two-phase refinement was performed with GSAS, using the structure reported by Peterson and Levy for D_2O.[24]

Table 1 lists the unit cell parameters of the ammonium compounds above and below T_N and at room temperature together with the *R* factors of Rietveld profile refinements, while the fractional coordinates and isotropic temperature factors have been deposited as supporting information. The equatorial oxygen atoms of the $M^{II}O_6$ groups are the four symmetry-related O(3) atoms which, due to their position off the (100) mirror plane, define a plane perpendicular to *bc*. In each octahedron, two O(3) atoms (referred to as the O(3a) atoms) are from the same phosphate group, and the remaining pair (O(3b)) are from adjacent phosphate groups. The O(3)−M−O(3) angles are all significantly distorted from 90°. However, the central metal ion is in all cases coplanar (within experimental error) with the equatorial oxygens, as can be determined by comparing the sum of the equatorial O−M−O angles with 360°. Of the apical oxygens, one (O(4)) is provided by the coordinated water molecule and is essentially perpendicular to the equatorial plane, while the remaining apex of the octahedron (O(1)) is occupied by a phosphate oxygen and is strongly distorted from the "vertical". The distortion of the octahedron can therefore be characterized by four angles: α, the O(3a)−M−O(3a) angle; β, the O(3a)−M−O(3b) angle (with O(3a) *cis* to O(3b)); γ, the O(3b)−M−O(3b) angle; and δ, the O(1)−M−O(4) angle. The refined values of these angles are summarized in Table 2, and they are shown pictorially in Figure 4, which indicates the equatorial plane and the projection of the $M^{II}O_6$ octahedron onto (100). Also defined in Figure 4a is ω, the angle which the equatorial plane of the octahedron makes with the (010) plane.

In all compounds, the M^{II}−O(1) and M^{II}−O(3b) bonds are shortened, while the M^{II}−O(2) and M^{II}−O(3a) bonds are lengthened. The angle α is significantly less than 90°, and β and γ are greater than 90° in compensation. The phosphate

(17) Pannetier, J. *Chem. Scr.* **1986**, *26A*, 131.
(18) Rietveld, H. M. *Acta Crystallogr.* **1967**, *22*, 151.
(19) Hewat, A. W. Report R7350; AERE: Harwell, U.K., 1973.
(20) Howard, C. J. *J. Appl. Crystallogr.* **1981**, *15*, 615.
(21) Cockcroft, J. K. Personal communication.
(22) Larson, A. C.; Von Dreele, R. B. Report LA-UR-86-748; Los Alamos National Laboratory; Los Alamos, NM, 1987.
(23) Durif, A.; Averbuch-Pouchot, M. T. *Bull. Soc. Fr. Mineral. Cristallogr.* **1968**, *91*, 495.
(24) Peterson, S. W.; Levy, H. A. *Acta Crystallogr.* **1967**, *A23*, 1948.

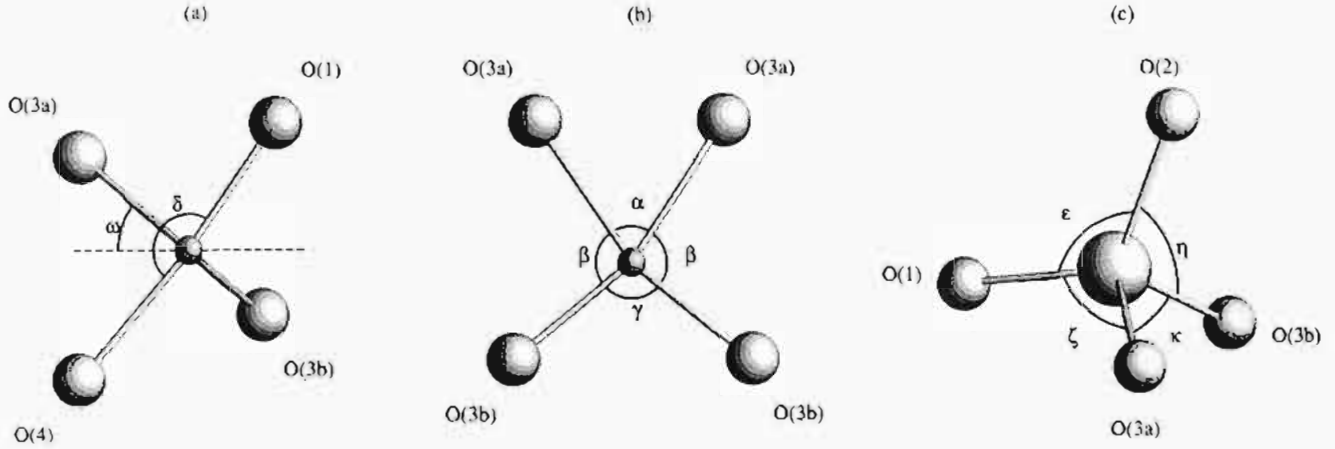

Figure 4. (a) Projection of the $M^{II}O_6$ group in $ND_4M^{II}PO_4{\cdot}D_2O$ onto (100) (the dashed line is parallel to the *c* axis). (b) Equatorial plane of $M^{II}O_6$. (c) PO_4, indicating symmetrically distinct bond angles.

Table 3. $M^{II}-O$ and P−O Bond Lengths (Å) in $ND_4M^{II}PO_4{\cdot}D_2O$ as a Function of Temperature and M^{II}

M^{II}	*T*/K	M−O(1)	M−O(4)	M−O(3a)	M−O(3b)	P−O(1)	P−O(2)	P−O(3)
Mn	1.6	2.123(9)	2.263(9)	2.279(7)	2.124(6)	1.520(12)	1.569(7)	1.556(6)
	21.4	2.114(8)	2.272(8)	2.258(6)	2.129(5)	1.529(10)	1.552(6)	1.557(5)
	298	2.116(8)	2.278(8)	2.374(6)	2.116(5)	1.534(10)	1.559(5)	1.548(5)
Fe	1.47	2.060(5)	2.261(5)	2.247(3)	2.044(3)	1.514(5)	1.556(5)	1.575(3)
	29.6	2.062(4)	2.265(3)	2.265(3)	2.029(3)	1.526(5)	1.530(6)	1.575(3)
	298	2.02(1)	2.23(1)	2.201(8)	2.081(7)	1.524(13)	1.558(7)	1.573(7)
Co	9.8	2.022(7)	2.203(7)	2.170(3)	2.067(3)	1.513(9)	1.547(5)	1.560(3)
	80	2.01(1)	2.22(1)	2.182(8)	2.063(7)	1.51(1)	1.552(7)	1.537(7)
	298	2.019(8)	2.191(8)	2.187(6)	2.055(5)	1.529(11)	1.575(6)	1.566(5)
Ni	9.8	2.048(4)	2.084(4)	2.160(3)	2.033(3)	1.520(5)	1.527(4)	1.559(3)
	80	1.985(9)	2.090(7)	2.141(5)	2.051(5)	1.540(11)	1.518(9)	1.561(6)
	298	1.995(5)	2.136(6)	2.181(5)	2.030(4)	1.519(6)	1.557(6)	1.548(5)

tetrahedron is also distorted, though to a lesser extent than the $M^{II}O_6$ octahedron. The phosphorus atom and two of the four oxygen atoms (O(1) and O(2)) lie in the *bc* mirror plane, while the two O(3) atoms are symmetry related by reflection in this plane. The bond angles are denoted by ϵ, ζ, η, and κ, referring to the O(1)−P−O(2), O(1)−P−O(3), O(2)−P−O(3), and O(3)−P−O(3) angles, respectively. Figure 4c defines the angles of the phosphate group, while the P−O bond lengths found in the ammonium metal phosphate hydrates are listed in Table 3, along with the $M^{II}-O$ bond lengths. In all cases except $ND_4NiPO_4{\cdot}D_2O$ at 80 K, the P−O(1) bond is distinctly shorter than P−O(2) and P−O(3), which are of similar lengths. The angle κ, subtended at phosphorus by the two O(3) atoms which are bonded to the same M^{II} ion, is invariably smaller than the remaining three O−P−O angles. The angle ϵ between the uncoordinated O(2) atom and the singly coordinated O(1) is also slightly smaller than the remaining two angles although in several cases the difference is comparable to the standard deviation.

The lengths of hydrogen bonds between the ammonium deuterons and the apical phosphate oxygens are listed in Table 4. The two hydrogen bonds between D(1) and D(2) and the two O(2) atoms in the (100) mirror plane (in two adjacent unit cells) are in the range 1.7−1.8 Å, while the two bonds between the D(3) deuterons and the O(2) atoms related by the ($^1/_2$ 0 $^1/_2$) glide plane are ~2.0 Å in length.

The $KM^{II}PO_4{\cdot}D_2O$ series of compounds have $M^{II}-PO_4-D_2O$ layers similar to those found in their ammonium analogues, but the layers are separated by K^+ instead of NH_4^+. Consequently, while there are no hydrogen bonds formed to the phosphate O(2), there are electrostatic interactions between this oxygen and the potassium ions. As a result of the smaller size of the potassium ion compared to ammonium, the interlayer separation

Table 4. O−D Bond Lengths (Å) in $ND_4M^{II}PO_4{\cdot}D_2O$ as a Function of Temperature and M^{II}

M^{II}	*T*/K	O(2)−D(1)	O(2)−D(2)	O(2)−D(3)
Mn	1.6	1.771(11)	1.734(11)	2.036(4)
	21.4	1.770(10)	1.755(10)	2.040(3)
	298	1.784(9)	1.746(10)	2.051(4)
Fe	1.5	1.741(6)	1.751(6)	2.023(3)
	29.6	1.771(10)	1.756(6)	2.032(3)
	298	1.750(13)	1.751(13)	2.017(4)
Co	9.8	1.734(8)	1.746(8)	2.010(2)
	80	1.734(13)	1.735(13)	1.998(4)
	298	1.757(10)	1.767(11)	2.014(3)
Ni	9.8	1.720(6)	1.761(6)	1.979(3)
	80	1.723(12)	1.745(11)	1.985(5)
	298	1.749(9)	1.763(9)	1.989(4)

Table 5. Unit Cell Constants (Å) and Profile Refinement Parameters of $KMnPO_4{\cdot}H_2O$ and $KM^{II}PO_4{\cdot}D_2O$ (M^{II} = Co, Ni)

M^{II}	*T*/K	*a*	*b*	*c*	R_{wp}	R_{exp}	R_I
Mn	1.7	5.6646(2)	8.2945(3)	4.8891(2)	12.78	4.25	8.56
	295	5.6768(2)	8.3358(4)	4.9058(2)	12.49	8.08	6.29
Co	80	5.5641(1)	8.2075(2)	4.7714(1)	2.83	2.55	11.41
	295	5.5835(1)	8.2558(2)	4.7964(1)	9.75	2.65	5.96
Ni	1.7	5.5281(1)	8.1806(2)	4.7269(1)	5.30	1.55	7.40
	3.9	5.5274(1)	8.1798(2)	4.7268(1)	5.54	2.18	7.86
	295	5.5372(1)	8.2166(2)	4.7445(1)	4.84	2.12	5.14

is smaller, as reflected in the *b*-axis parameter. Table 5 contains the unit cell constants and Rietveld profile refinement parameters for the K series, while the fractional atomic coordinates and isotropic temperature factors have been deposited as supporting information. Refined bond lengths and angles of the $M^{II}O_6$ octahedra and the PO_4 tetrahedra will be found in Tables 6 and 7. Again, the O(3a)−M^{II}−O(3a) bond angle is significantly

Table 6. M^{II}–O and P–O Bond Lengths (Å) in $KMn^{II}PO_4{\cdot}D_2O$ as a Function of Temperature and M^{II}

M^{II}	*T*/K	M–O(1)	M–O(4)	M–O(3a)	M–O(3b)	M–O–M	P–O(1)	P–O(2)	P–O(3)
Mn	1.5	2.125(8)	2.262(8)	2.278(6)	2.131(5)	116.7(2)	1.521(10)	1.486(7)	1.594(5)
	298	2.084(8)	2.319(8)	2.283(7)	2.119(6)	117.5(2)	1.551(15)	1.516(9)	1.576(7)
Co	80	2.048(9)	2.198(9)	2.228(7)	2.029(6)	119.4(3)	1.541(6)	1.500(6)	1.576(4)
	298	2.063(6)	2.168(5)	2.221(5)	2.054(4)	119.6(2)	1.537(4)	1.532(4)	1.565(3)
Ni	1.7	2.013(5)	2.110(5)	2.156(4)	2.045(3)	120.4(1)	1.529(7)	1.548(6)	1.567(4)
	3.9	2.035(4)	2.099(5)	2.150(4)	2.049(3)	120.5(1)	1.506(6)	1.540(6)	1.566(4)
	298	2.034(4)	2.106(6)	2.177(4)	2.037(3)	120.2(1)	1.510(6)	1.549(6)	1.576(4)

Table 7. O–M^{II}–O (α, β, γ, δ) and O–P–O (ϵ, ζ, η, κ) Bond Angles (deg) in $KM^{II}PO_4{\cdot}D_2O$ as a Function of Temperature and M^{II} [a]

M^{II}	*T*/K	α	β	γ	$(\alpha + 2\beta + \gamma)$	δ	ϵ	ζ	η	κ
Mn	1.7	65.5(2)	98.6(1)	97.2(2)	359.9(6)	174.7(3)	111.9(5)	110.2(4)	111.4(3)	101.4(4)
	298	66.0(2)	98.1(2)	98.1(2)	359.9(8)	175.5(3)	110.1(7)	109.6(5)	111.6(5)	104.2(6)
Co	80	67.8(2)	96.7(1)	98.7(4)	359.9(8)	173.5(4)	110.0(4)	110.1(3)	111.3(3)	104.1(3)
	298	67.4(2)	96.9(1)	98.8(2)	360.0(6)	174.5(3)	110.9(3)	110.5(2)	110.4(2)	103.9(2)
Ni	1.7	70.0(1)	96.7(1)	96.7(1)	360.1(4)	176.6(2)	109.5(4)	111.1(3)	110.5(2)	104.1(3)
	3.9	70.0(1)	96.7(1)	96.7(1)	360.1(4)	176.8(2)	108.5(4)	112.0(3)	110.2(2)	103.9(3)
	298	69.9(1)	96.7(1)	96.7(2)	360.0(4)	176.4(2)	109.7(4)	111.3(3)	109.9(2)	104.6(3)

[a] For definition of the angles, see Figure 4.

less than 90°, while the remaining equatorial bond angles are greater than 90°. The relative lengths of the M^{II}–O bonds show the same distortions as in the ammonium compounds, with M^{II}–O(1) and M^{II}–O(3b) shorter than M^{II}–O(2) and M^{II}–O(3a). In the phosphate tetrahedron, the P–O(3) bond remains the longest, though the relative lengths of the P–O(1) and P–O(2) bonds show no clear pattern. The angle κ is invariably smaller than the remaining three angles, which show no consistent order of size.

Magnetic Structure Determinations. In the low-temperature neutron diffraction powder profiles of $ND_4M^{II}PO_4{\cdot}D_2O$ (M^{II} = Mn, Fe, Co, Ni), $KMnPO_4{\cdot}H_2O$, and $KM^{II}PO_4{\cdot}D_2O$ (M^{II} = Co, Ni), both of the Mn compounds and the Fe compound showed strong magnetic scattering which could be indexed to the nuclear unit cell. However, in the diffraction patterns of the Co and Ni compounds, the magnetic scattering was very weak, with nonintegral Miller indices which were difficult to index unambiguously. Thus we treat the Mn and Fe examples in greatest detail.

Bertaut has shown that some of the possible magnetic structures compatible with a given space group can be predicted from symmetry arguments.[25] This method is particularly useful if the magnetic and chemical unit cells are coincident, as is the case for the ternary Mn and Fe phosphates. Bertaut's so-called method of irreducible representations was therefore applied to the space group $Pmn2_1$ with the following results:

mode	invariant representations
A_1	A_x
A_2	F_y, A_z
B_1	A_y, F_z
B_2	F_x

where "A" indicates spin reversal between the two metal ions in the unit cell, "F" indicates no spin reversal, and the subscripts indicate the axis along which the spin component lies.

Thus there are two possible representations in which antiferro- and ferromagnetic moments can coexist. Rietveld refinements show clearly that in all three compounds the B_1 mode describes the actual magnetic structure, with the antiferromagnetic moments along [0 ±1 0] and the ferromagnetic moments along [001]. These are described by the magnetic rotation matrix

$$\mathbf{M} = \begin{pmatrix} 0 & 0 & 0 \\ 0 & -1 & 0 \\ 0 & 0 & 1 \end{pmatrix} \quad (1)$$

acting on the moment vector

$$\mathbf{k} = \begin{pmatrix} 0 \\ M_a \\ M_f \end{pmatrix} \quad (2)$$

Unfortunately, the magnitude of the canting is too small to allow the ferromagnetic moment to be resolved from the data available. The antiferromagnetic structure of the three compounds is illustrated in Figure 5, and the parameters of the magnetic refinements of the 1.6(1) K profiles are as follows:

$ND_4MnPO_4{\cdot}D_2O$: $M_y = 4.64(4)\,\mu_B$; $R_{mag} = 7.15\%$

$ND_4FePO_4{\cdot}D_2O$: $M_y = 4.22(3)\,\mu_B$; $R_{mag} = 8.47\%$

$KMnPO_4{\cdot}H_2O$: $M_y = 4.16(3)\,\mu_B$; $R_{mag} = 10.48\%$

(The nuclear coordinates obtained from these refinements are listed in the supporting information.) The form factors used in the refinements were those calculated by Freeman and Watson.[26]

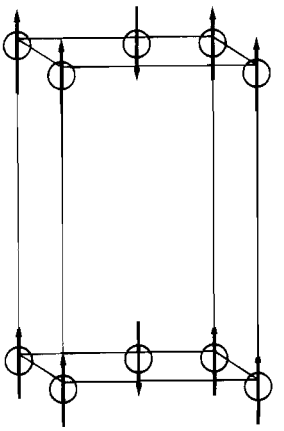

Figure 5. Antiferromagnetic structure of $M^IM^{II}PO_4{\cdot}D_2O$ (M^{II} = Mn, Fe).

(25) Bertaut, E. F. *Acta Crystallogr.* **1968**, *A24*, 217.

(26) Freeman, A. J.; Watson, R. E. *Acta Crystallogr.* **1961**, *14*, 234.

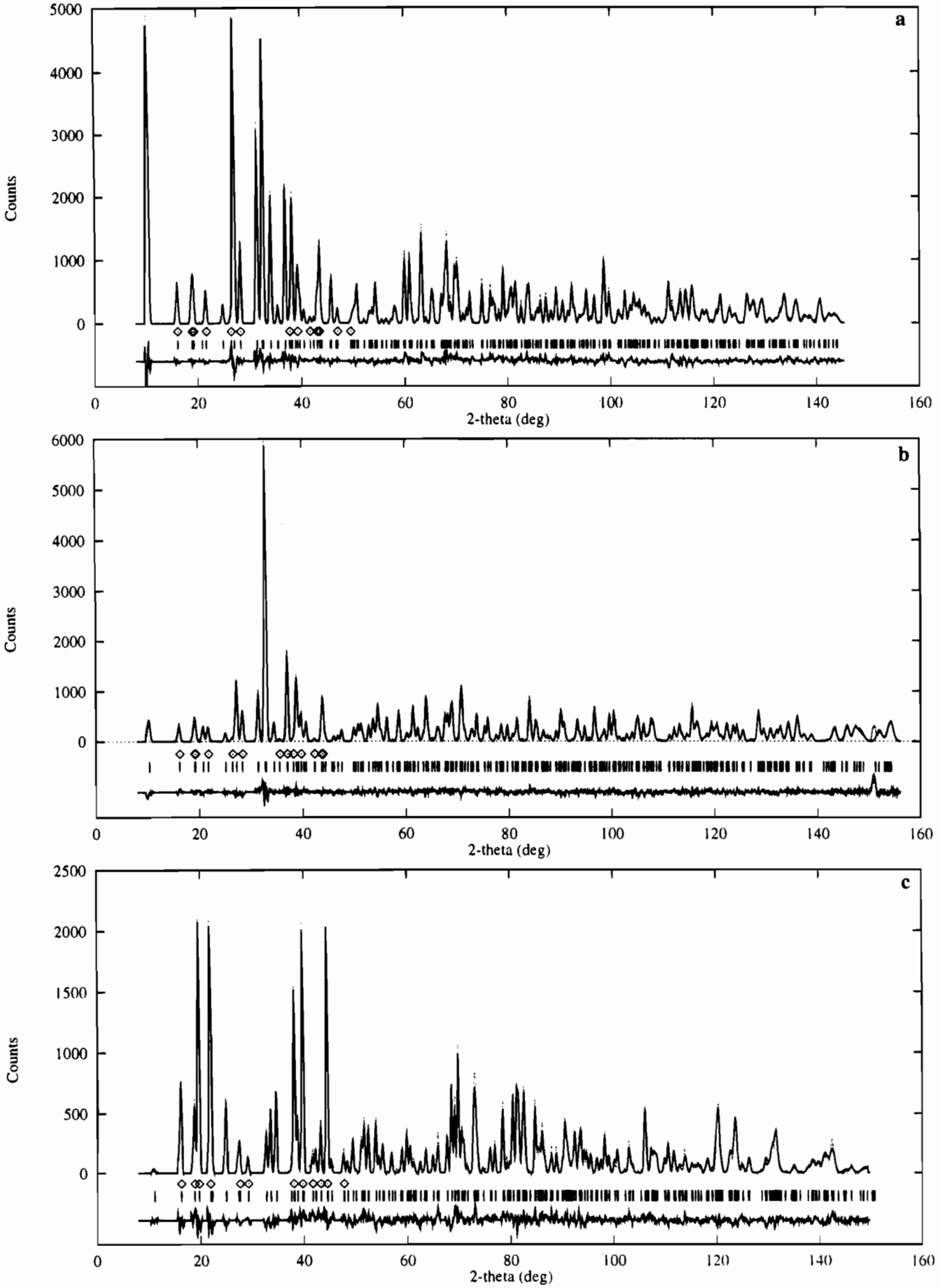

Figure 6. Observed (points), calculated (upper full line), and difference (lower full line) neutron powder diffraction profiles of $ND_4M^{II}PO_4 \cdot D_2O$ (M^{II} = Mn (a), Fe (b)) and $KMnPO_4 \cdot H_2O$ (c) at 1.6 K. Bars indicate nuclear reflections, and diamonds, magnetic reflections.

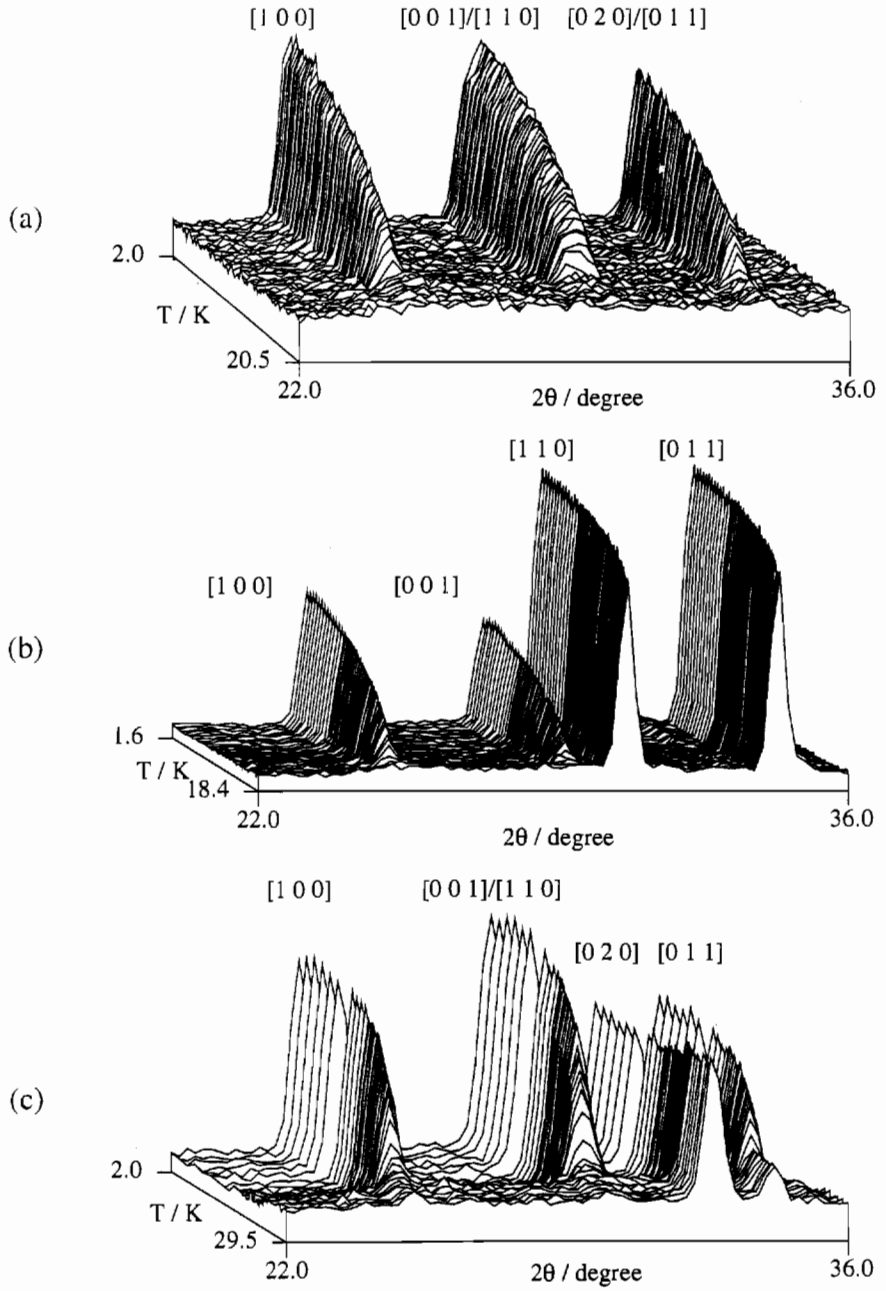

Figure 7. Low-angle neutron powder diffraction peaks of $ND_4M^{II}PO_4{\cdot}D_2O$ (M^{II} = Mn (a), Fe (b)) and $KMnPO_4{\cdot}H_2O$ (c) as a function of temperature.

Observed, calculated, and difference profiles for the three magnetic refinements are shown in Figure 6.

Neutron powder diffraction profiles of $M^IMnPO_4{\cdot}D_2O$ (M^I = K, ND_4) and $ND_4FePO_4{\cdot}D_2O$ measured as a function of temperature in the low-scattering-angle region are shown in Figure 7. In each compound, the (100) and (001) reflections are purely magnetic, as they are systematic absences of space group $Pmn2_1$. The (110) and (011) reflections have both magnetic and nuclear contributions to their intensity (the nuclear components are weak in the ammonium compounds but strong in $KMnPO_4{\cdot}H_2O$). The intensities of the magnetic reflections were fitted to a model consisting of a Gaussian peak with a parabolic background from which the ordering temperatures T_N were estimated to be as follows: for $ND_4MnPO_4{\cdot}D_2O$, 17.5(3) K; for $KMnPO_4{\cdot}H_2O$, 18.0(3) K; and for $ND_4FePO_4{\cdot}D_2O$, 24.0(2) K. The phase transition in the Fe compound is clearly second order, not first order as reported earlier.[13] From the temperature dependence of the magnetic scattering intensity it is possible to extract values of the critical exponent β in the expression where $\epsilon = (T_N - T)/T_N$. This has been done in the case of $ND_4MnPO_4{\cdot}D_2O$, and the results have been compared with those obtained from bulk magnetization measurements. There is a crossover in the exponent at $\epsilon \sim 0.030(5)$ from 0.20(1) to 0.39(4).[27]

Magnetic Ordering in Co and Ni Compounds. Magnetic Bragg scattering was observed in the low-temperature profiles of three compounds; $M^ICoPO_4{\cdot}D_2O$ (M^I = K, NH_4) and $ND_4NiPO_4{\cdot}D_2O$. It was very weak, and although it is clear that the magnetic and chemical unit cells are not coincident, the nature of the ordering has not yet been determined. Profiles of the two ND_4 compounds measured above and below T_N, with different plots revealing the magnetic reflections, are shown in Figure 8, and suggested assignments for the observed magnetic reflections are listed in Table 8.

Susceptibility Measurements. The magnetic susceptibility of $NH_4FePO_4{\cdot}H_2O$ over the range 4.2−300 K has been described by Greedan *et al.*[13] The temperature dependence of the

(27) Carling, S. G.; Day, P.; Visser, D. *Solid State Commun.* **1993**, *88*, 135.

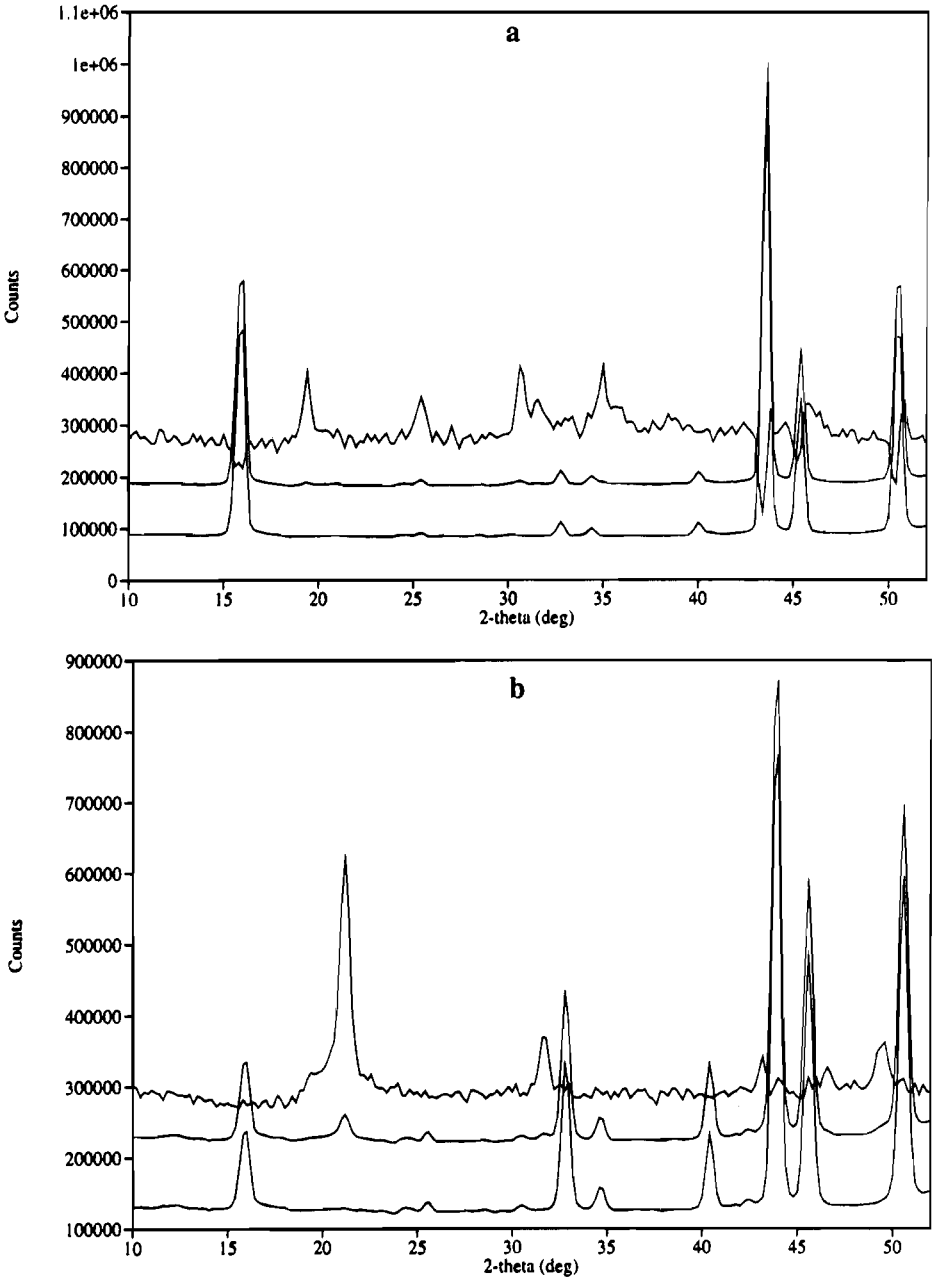

Figure 8. Neutron powder diffraction profiles of $ND_4M^{II}PO_4{\cdot}D_2O$ (M^{II} = Co (a), Ni (b)): bottom, 9.3 K; center, 1.6 K; top, difference (20 times enlarged).

Table 8. Observed and Calculated Magnetic Reflections in $M^IM^{II}PO_4{\cdot}D_2O$ (*d* Spacings/Å)

	$ND_4CoPO_4{\cdot}D_2O$		$KCoPO_4{\cdot}D_2O$		$ND_4NiPO_4{\cdot}D_2O$	
	obs	calc	obs	calc	obs	calc
1/2 0 1/2	7.46	7.20			7.46	7.27
1/2 1/2 1/2			6.78	6.63		
1/2 1 0					6.83	6.88
1/2 1 1/2	5.64	5.60	5.27	5.43		
1 1/2 1/2	4.71	4.66			4.57	4.62
1/2 3/2 1/2	4.57	4.56	4.37	4.37	4.57	4.54
1/2 2 0	4.13	4.09				
1 3/2 0	4.05	4.05				

susceptibility of $M^IMnPO_4{\cdot}H_2O$ (M^I = NH_4, K) is shown in Figures 9 and 10. Both compounds show Curie–Weiss behavior above 80 K, with deviations due to short-range order below this temperature. A broad maximum, characteristic of 2D antiferromagnetism, is seen in the susceptibilities of both compounds above the onset of long-range order at T_N. The temperature at which this maximum occurs is related to the exchange constant, *J*, as follows:[28]

$$\tau_m = \frac{k_B T(\chi_{max})}{|J|S(S+1)} \tag{3}$$

For a square-planar, Heisenberg antiferromagnet with $S = {}^5/_2$, $\tau_m = 2.06(3)$. No such simple analysis is available for a 2D rectangular lattice, but since the deviation from square planar in our compounds is not very great and there is only one exchange path, we have used the square-planar model.

Results of fits to the Curie–Weiss law and other quantities derived from the analysis of the bulk susceptibility data are given in Table 9. The value of μ_{eff} shown for $NH_4MnPO_4{\cdot}H_2O$ in this table is slightly higher than the expected "spin-only" value of 5.92 μ_B, as is the value calculated for the corresponding K compound using the 1.0 T data. The lower field data give a

(28) Navarro, R. In *Magnetic Properties of Layered Transition Metal Compounds*; de Jongh, L. J., Ed.; Kluwer Academic Publishers: Dordrecht, The Netherlands, 1990.

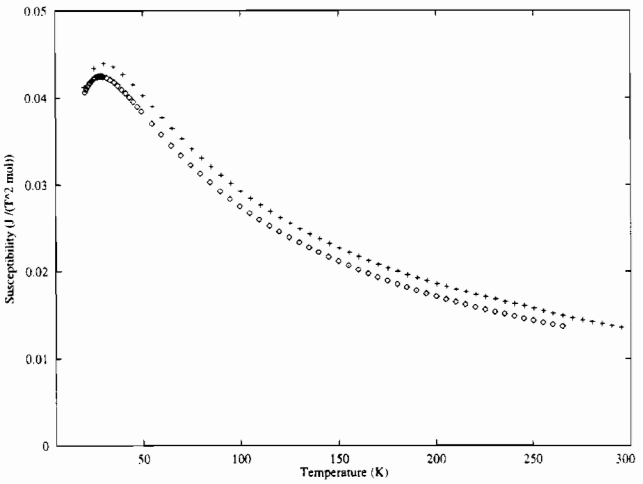

Figure 9. Bulk susceptibility above T_N of $KMnPO_4{\cdot}H_2O$ (crosses) and $NH_4MnPO_4{\cdot}H_2O$ (diamonds) measured in a field of 50 mT.

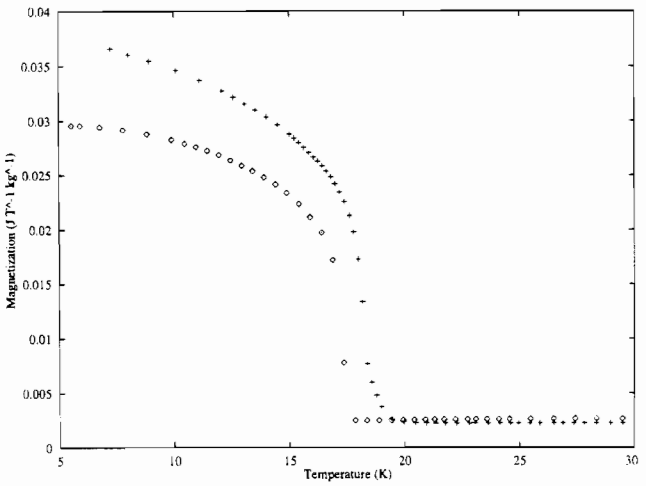

Figure 10. Low-temperature magnetization of $KMnPO_4{\cdot}H_2O$ (crosses) and $NH_4MnPO_4{\cdot}H_2O$ (diamonds) measured in a field of 10 mT.

Table 9. Magnetic Parameters of $M^IMnPO_4{\cdot}H_2O^a$

M^I	T_N/K	$T(\chi_{max})$/K	C/emu K mol^{-1}	Θ/K	μ_{eff}/μ_B	(J/k)/K
NH_4	17.5(1)	29.0(5)	4.536(6)	−65.1(3)	6.049(8)	−1.61(4)
K[a]	18.4(3)	29.8(5)	3.56(1)	−62.7(7)	5.36(2)	−1.66(4)
K[b]	18(1)	27(2)	4.73(6)	−61(2)	6.18(8)	−1.66(4)

[a] 0.05 T, SQUID. [b] 1.0 T, Faraday balance.

significantly lower μ_{eff}, perhaps due to inaccuracy in the weight of the sample.

Discussion

Crystal Chemistry. Although the unit cell parameters of all the phosphates show some variation with temperature, their cell volumes are approximately constant for a given M^IM^{II} pair at all temperatures studied, the difference between the smallest and largest volume found being less than 1% in all cases. The trend is for increasing unit cell volume with increasing temperature in all cases but two: both $ND_4MnPO_4{\cdot}D_2O$ and $ND_4FePO_4{\cdot}D_2O$ show a slight decrease in volume above their Neel temperatures. While the magnitude of this decrease is small (0.4 Å^3 for the former, 0.3 Å^3 for the latter), it is accompanied by more marked variations in their cell axes (Table 1), almost certainly a consequence of magnetostriction due to the weak ferromagnetism in the ordered state. In contrast, for a given M^I, there is a marked variation of cell volume with the divalent metal ion. In the ammonium compounds, the trend is readily accounted for by the decrease in ionic radius of the first transition series ions, as may be seen from Table 3, which shows the average length of the M−O bonds in the $M^{II}O_6$ octahedron. In the potassium materials however, the average M−O bond lengths are approximately the same for cobalt and nickel, the Co−O bonds being shorter than those in the ammonium analogue. The smaller cell volumes of the potassium compounds are a consequence of their smaller interlayer separation.

While the overall dimensions of the $M^{II}O_6$ octahedron are a function of the radius of the divalent ion, its distortion and orientation are determined by the necessity of forming a cross-linked structure with the phosphate group, which is essentially a rigid moiety. Thus if the phosphate group moves away from the metal ion which it coordinates in a bidentate manner, the M−O(3a) bond length increases and at the same time the O(3a)−M−O(3a) bond angle (denoted α in Figure 4) decreases. At the same time, the bonds these oxygen atoms form to the adjacent metal ions (the M−O(3b) bonds) decrease in length and the O(3b)−M−O(3b) bond angle (β in Figure 4) increases. Such a trend is indeed apparent in the data of Tables 3 and 7.

Magnetic Structures. The symmetry of space group $Pmn2_1$ is sufficiently low to allow antisymmetric exchange, as proposed by Moriya,[7] which would account for the weak ferromagnetism observed. The exchange, which operates in addition to the isotropic Heisenberg exchange, is described on a microscopic level by the equation

$$\mathcal{H}_{aniso} = \mathbf{d}_1[\mathbf{s}_1 \times \mathbf{s}_2] \quad (4)$$

It derives from the anisotropic spin interaction, described as the sum of symmetric and antisymmetric components

$$V_{1,2} = \mathbf{s}_1{\cdot}\mathbf{K}_S{\cdot}\mathbf{s}_2 + \mathbf{s}_1{\cdot}\mathbf{K}_A{\cdot}\mathbf{s}_2 \quad (5)$$

where the symmetric and antisymmetric tensors $\mathbf{K}_S$ and $\mathbf{K}_A$ are approximated by

$$\mathbf{K}_S \sim (\lambda/\Delta)^2 J \sim (\Delta g/g)^2 J \quad (6)$$

$$\mathbf{K}_A \sim (\lambda/\Delta) J \sim (\Delta g/g) J \quad (7)$$

In these equations λ is the spin−orbit coupling, Δ is the ligand field splitting, and $\Delta g = g - 2$. To a first approximation, the ground state of Mn^{2+} is $^6S_{5/2}$, and the ion should therefore be isotropic. In a crystal field, however, second-order spin−orbit coupling mixes the $^4T_{1g}$ excited state into the $^6A_{1g}$ ground state, resulting in deviations of g from the free-spin value.[29] Additionally, in compounds where there is a degree of covalent bonding, ligand−metal charge transfer can result in admixture of further excited states, which can also cause shifts in g.[30,31]

Moriya also describes constraints on the direction of the vector **d** imposed by crystal symmetry.[7] In the case of the compounds described here, the symmetry operation which relates the metal centers of the two sublattices is the ($^1/_2$ 0 $^1/_2$) glide plane, and **d** is therefore constrained to lie parallel to this plane. This is compatible with the magnetic structure determination using Bertaut's method of irreducible representations,[25] from which we concluded that the weak ferromagnetic moment must lie parallel to the crystallographic c axis.

It is clear that the underlying antiferromagnetic structures of the two Mn compounds and the Fe compound are the same. Unfortunately the canting of the moments responsible for the weak ferromagnetism of these materials is too small to be

(29) Watanabe, H. *Prog. Theor. Phys.* **1957**, *18*, 405.
(30) Fidone, I.; Stevens, K. W. H. *Proc. R. Soc. London* **1959**, *73*, 116.
(31) Watanabe, H. *J. Phys. Chem. Solids* **1964**, *25*, 1471.

resolved with powder neutron data. However, an estimate of the weak antiferromagnetic moment can be obtained from our remnent field magnetization measurements. The bulk magnetization measured in the remnent field at the lowest temperature (~5 K) may be converted to a moment according to the equation

$$\mu_{\text{ferro}} = \frac{M(T)}{M_R \cdot N_A \cdot \mu_B} \tag{8}$$

If $M(T)$ is in units of A m^2 kg^{-1} and M_R is in kg mol^{-1}, then the moment is in μ_B $atom^{-1}$. The values of μ_{ferro} calculated in this manner are 3.4(1) $\times$ 10^{-3} μ_B $atom^{-1}$ for $NH_4MnPO_4 \cdot H_2O$ and 3.5(1) $\times$ 10^{-3} μ_B $atom^{-1}$ for the corresponding K compound. It is important to note that these values represent a lower limit to the weak ferromagnetic moment, as the antiparallel alignment of domains in the sample will tend to reduce the net moment.

Conclusions

Neutron powder diffraction has enabled us to determine the crystal structures of the isomorphous series of layer compounds $KM^{II}PO_4 \cdot D_2O$ and $ND_4M^{II}PO_4 \cdot D_2O$ (M^{II} = Mn, Fe, Co, Ni) and define the distortion of the $M^{II}O_6$ coordination polyhedron as a function of M^{II} and temperature. The network of H-bonds knitting together the $M^{II}-PO_4-D_2O$ layers in the ammonium compounds has also been resolved. At low temperatures, all the compounds behaved as canted antiferromagnets and the underlying antiferromagnetic structures of the Mn and Fe compounds have been refined, though the neutron powder data do not permit any estimate of the canting angle. However bulk magnetization data measured in the remnent field of a superconducting magnet suggest a canted moment of ~3.5 $\times$ 10^{-3} μ_B $atom^{-1}$ in the Mn compounds. The close similarity between the magnetic parameters T_N and μ_{ferro} of $M^IMnPO_4 \cdot H_2O$ for M^I = NH_4 and K demonstrates that the network of H-bonds connecting the magnetic layers together in the ammonium compound has little influence on interlayer interaction. Nevertheless, distorted metal ion coordination and low-symmetry crystal structures are clearly a fruitful source of weakly ferromagnetic low-dimensional lattices.

Acknowledgment. We thank the U.K. Science and Engineering Research Council for a Research Grant and an Earmarked Studentship (S.G.C.) under the 21st Century Materials Initiative. We are grateful to the Institut Laue Langevin, Grenoble, France, for provision of beam time and Dr. J. K. Cockcroft for his help and advice.

Supporting Information Available: Tables of atomic coordinates and thermal parameters and figures showing neutron diffraction profiles (14 pages). Ordering information is given on any current masthead page.

IC941435O